Plasmon Inducing Effects for Enhanced Photoelectrochemical Water Splitting: X-ray Absorption Approach to Electronic Structures

Hao Ming Chen,[†,‡] Chih Kai Chen,[†] Chih-Jung Chen,[†] Liang-Chien Cheng,[†] Pin Chieh Wu,[∥] Bo Han Cheng,[§] You Zhe Ho,[‡] Ming Lun Tseng,[∥] Ying-Ya Hsu,[¶] Ting-Shan Chan,[⊥] Jyh-Fu Lee,[⊥] Ru-Shi Liu,[†,*] and Din Ping Tsai[‡,#,*]

[†]Department of Chemistry and [‡]Department of Physics, National Taiwan University, Taipei 106, Taiwan, [§]Institute of Electro-Optical Science and Engineering, National Cheng Kung University, Tainan 701 Taiwan, [¶]Program for Science and Technology of Accelerator Light Source, National Chiao Tung University, Hsinchu 300, Taiwan, [⊥]National Synchrotron Radiation Research Center, Hsinchu 300, Taiwan, [#]Research Center for Applied Sciences, Academia Sinica, Taipei 115, Taiwan, and [∥]Graduate Institute of Applied Physics, National Taiwan University, Taipei 106, Taiwan

ABSTRACT Artificial photosynthesis using semiconductors has been investigated for more than three decades for the purpose of transferring solar energy into chemical fuels. Numerous studies have revealed that the introduction of plasmonic materials into photochemical reaction can substantially enhance the photo response to the solar splitting of water. Until recently, few systematic studies have provided clear evidence concerning how plasmon excitation and which factor dominates the solar splitting of water in photovoltaic devices. This work demonstrates the effects of plasmons upon an Au nanostructure—ZnO nanorods array as a photoanode. Several strategies have been successfully adopted to reveal the mutually independent contributions of various plasmonic effects under solar irradiation. These have clarified that the coupling of hot electrons that are formed by plasmons and the electromagnetic field can effectively increase the probability of a photochemical reaction in the splitting of water. These findings support a new approach to investigating localized plasmon-induced effects and charge separation in photoelectrochemical processes, and solar water splitting was used herein as platform to explore mechanisms of enhancement of surface plasmon resonance.

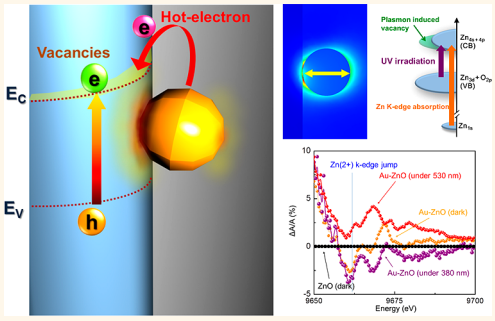

KEYWORDS: plasmon · water splitting · X-ray absorption spectroscopy · gold · zinc oxide

The meeting of future demand for energy without the combustion of fossil fuels depends on the efficient production of solar energy. The photolysis of water using semiconductor materials has been investigated as a clean process for converting renewable energy by storing solar energy in chemical bonds such as those of hydrogen. Hydrogen that is formed by the splitting of water using solar energy is clearly attractive as a clean energy vector, and various attempts have been made to construct viable molecular and biomolecular devices for producing hydrogen.[1−5] The basis of photosynthesis, on which the existence of various life-forms on Earth depend, is a remarkable chemical reaction, in which solar energy converts water and carbon dioxide into chemical fuel and oxygen. The development of an artificial mechanism of photosynthesis, based on splitting water into hydrogen and oxygen, to meet future demand for energy, is greatly desired.[6] Since Honda and Fujishima elucidated the possibility of splitting water using titania, various semiconductor materials have been demonstrated to exhibit photoactive properties in the water-splitting reaction or half-reaction.[7−12] The photochemical process of splitting water involves the excitation of a material such as oxide semiconductor with photons of higher energy than the bandgap, to generate electron−hole pairs, which either recombine or react with an adsorbed species. An effective photovoltaic device is one that can use these electrons and holes efficiently to generate hydrogen and/or oxygen before recombination can occur.

Recently, the field of plasmonics has expanded rapidly because of the easiy tailoring and shape-dependent optical properties of the plasmonics.[13−19] Many materials and devices have been found to have several plasmonic applications, such as plasmonics lasers,[20] surface-plasmon-enhanced light-emitting diodes,[21] metamaterials,[22,23] plasmon focusing,[24] plasmon waveguides,[25] and others.[26−30] Lately, some investigations

* Address correspondence to rsliu@ntu.edu.tw, dptsai@sinica.edu.tw.

Received for review June 5, 2012 and accepted July 31, 2012.

Published online July 31, 2012
10.1021/nn3024877

have found that introducing plasmonic materials into a photochemical reaction can markedly enhance the photo response to the solar water splitting mechanism of this enhancement, which has been proposed to involve either charge transfer between metal and oxide (by so-called "hot" electron−hole pairs) or plasmon-induced heating and establishment of an electromagnetic field.[31−37] Despite proposals of such mechanisms, until recently, few systemic studies have provided any evidence concerning them or information concerning how plasmon excitation and which domination factor in photovoltaic devices for solar water splitting. Understanding the mechanism of plasmonic enhancement is a crucial aspect and is useful for future development of photovoltaic devices. However, distinguishing among independent photoresponses to solar radiation associated with various plasmonic effects is a key challenge.

To elucidate the plasmonic enhancement mechanism, independent plasmon-induced photoresponses must be distinguished from each other in the overall photochemical signal of water splitting. This challenge is overcome herein using three important strategies. First, a photoelectrochemical cell (PEC) is used as a platform rather than a photocatalyst in evaluating photoactivity, since a PEC can directly extract an electrical signal from photoactive materials upon irradiation without the need for measuring the production of gas. The splitting of water into hydrogen and oxygen directly by sunlight in a PEC is an ideal method for producing hydrogen that integrates solar energy collection with water electrolysis at a single photoelectrode. Accordingly, a PEC enables independent photoresponses to be associated with recognizable plasmonic effects. Second, a plasmonic photoelectrode is measured with polarized illumination along various axes because of the polarization-dependent localized plasmon oscillation; these measurements can be easily combined with a theoretical simulation to evaluate a plasmon-induced effect. Third, since localized plasmonic oscillation generates an electromagnetic field upon the surface of plasmon materials, modifying the plasmon metal/semiconductor interface, it may alter the electronic structure of the semiconductor and thereby generate a localized transition state. X-ray absorption spectroscopy (XAS), which is sensitive to the electronic structures and local structures of nanomaterials, has been applied to various metal or oxide semiconductors.[38−41] The use of monochromatic radiation makes XAS element-selective and therefore highly effective when used on samples that contain more than one species of metal atom, or substrate lattices, which interfere with diffraction measurement. The *in situ* X-ray absorption spectroscopy was carried out in fluorescence mode to determine the evolution of the electronic structure that is caused by localized plasmonic effects because of the sensitivity of the fluorescence signals to surface, This evolution can be used to elucidate the electronic modification of ZnO at the surface.[42,43] Likewise, the X-ray absorption spectrum can be obtained *in situ* under monochromatic illumination and an applied bias, and the transfer of photogenerating electrons under irradiation by monochromatic incident light can be elucidated.

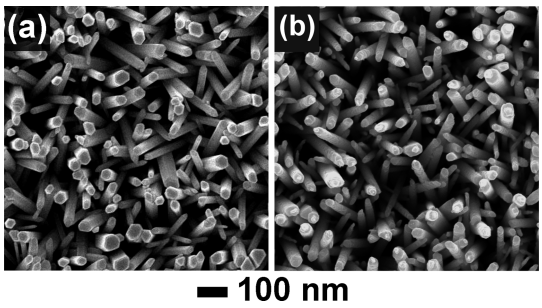

Figure 1. SEM images of bare ZnO (a) and Au−ZnO photoelectrodes with nanoparticles deposited for 12 h deposition (b).

In this work, a photoelectrode in the form of an array of ZnO nanorods was prepared and decorated with various amounts of plasmonic gold nanospheres, and its photoelectrochemical activity was investigated. Several strategies were utilized to elucidate the relationship between the photoresponse and underlying plasmon-induced effects, such as hot-electron injection, the generation of an electromagnetic field, and heating. *In-situ* X-ray absorption spectroscopy elucidated the evolution of the electronic structure following localized plasmonic effects, and theoretical simulations based on the finite element method (FEM) also elucidated plasmon-induced effects.

RESULTS AND DISCUSSION

In this study, an array of ZnO nanorods was prepared with various amounts of plasmonic gold nanospheres as a platform to examine the plasmon-induced effects on a photoelectrode in the splitting of water. One-dimensional nanorods have been demonstrated to be efficient in photoelectrochemical (PEC) cell and photovoltaic cell applications because they can decouple the direction of light absorption and charge carrier collection.[44−48] Nanorods have a small radius, and minority carriers that are generated therein can diffuse to their surfaces before they recombine. This effect increases charge separation efficiency, especially when the minority carrier diffusion length is comparable to the radius of the nanorod. Additionally, the shape of a plasmonic gold nanostructure has been demonstrated to be easily controlled using numerous methods and the also exhibit strongly shape-dependent optical properties,[17,18] meaning that present investigation can considerably operate in other systems. An array of ZnO nanorods was synthesized over the surface of SnO_2:F (FTO) glass substrate using the hydrothermal method. Figure 1 characterizes the nanostructures of

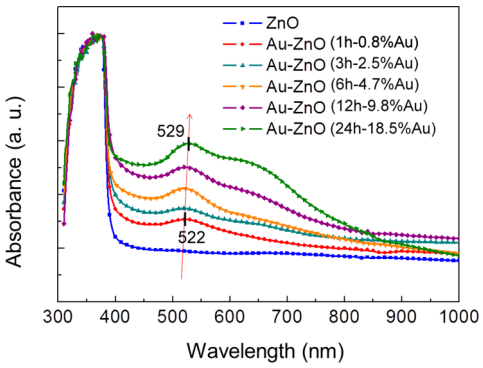

Figure 2. Absorption spectra of Au−ZnO photoelectrodes with Au nanoparticles deposited over various periods.

an array of ZnO nanorods and an Au−ZnO electrode with plasmonic gold nanoparticles that had been deposited for 12 h. Scanning electron microscopic (SEM) images present the growth of dense and vertically aligned ZnO nanorods on the FTO substrate; the typical length is ~5 μm (Supporting Information, Figure S1). As the duration of deposition increases to 24 h, the morphology of ZnO nanorods does not significantly change (Supporting Information, Figure S2). Notably, the surface of ZnO that had been deposited with Au nanoparticles for 24 h was slightly rough owing to the formation of a thin layer of Au nanoparticles upon it. Since the particles size were very small (less than 5 nm), further structural characterization was conducted using a transmission electron microscope (*vide infra*).

Localized surface plasmon resonances, which are caused by the interaction of incident light with gold nanoparticles, are well-known to be effective in for biological sensors, surface-enhanced Raman spectroscopy, and optical devices,[49,50] because the wavelength of plasmon resonance depends strongly on the structure and composition of the material, and the local dielectric environment. Gold nanostructures serve as a platform in this investigation, and are used to reveal plasmon-induced effects on a semiconductor, because their resonant wavelength is in the visible region rather than in the ultraviolet, and so overlap with the wavelengths absorbed by of a wide bandgap semiconductor (ZnO). Optical spectra of Au−ZnO photoelectrodes on which Au nanoparticles had been deposited for various times exhibited a clear increase in absorbance corresponding to the gold nanospheres in addition to strong ultraviolet absorption of ZnO (Figure 2). As deposition time increased, the absorbance that originated in the surface plasmon resonance of gold nanoparticles (at approximately 530 nm) considerably increased, suggesting that the gold nanoparticle loading could be effectively controlled by varying the deposition duration and conditions, enabling the conditions of the photoelectrochemical reaction to be optimized. Compared to the absorption spectrum of Au nanoparticles in aqueous solution (Supporting Information, Figure S3), the deposition Au nanoparticles on the ZnO surfaces were accompanied by a red shift in a surface plasmon peak continuously toward the red region. The red shift from 522 to 529 nm is attributed to the progressive deposition of Au particles upon the ZnO. This peak shift may have been caused by the dielectric variance of the surrounding environment and interparticle distance upon the gold nanoparticles.[51] Supporting Information, Table S1 shows the elemental analysis of Au−ZnO photoelectrodes from inductively coupled plasma atomic emission spectrometer, which reveals that chemical bath deposition can modify the gold nanoparticles upon the surface of ZnO and significantly control the loading amount of plasmonic materials. The absorption spectra reveal that gold nanoparticles were successfully attached to the surface of the ZnO nanorods array during the chemical bath deposition, but not by physical methods, since the deposition of a monolayer can clearly reveal localized surface plasmon effects without causing any undesired effects. Notably, the absorption spectrum obtained at a deposition time of 24 h included a peak at approximately 650 nm in addition to the major plasmon resonance peak. This phenomenon is attributable to the formation of clusters aggregation that was composed of gold nanoparticles.[51]

Electrochemical measurements were made systematically to evaluate the photoelectrochemical properties of ZnO nanowires that were loaded with Au nanoparticles. Figure 3a shows a set of linear sweep voltammagrams of pristine ZnO nanorods and ZnO nanorods that were loaded with Au nanoparticles that had been deposited for various durations under 100 mW/cm^2 of illumination. A dark scan from −0.5 to +1.1 V revealed a small current of around 10^{-6} A/cm^2. The photocurrent increased dramatically with deposition time to 12 h. ZnO nanorods with loading of 12 h yielded a pronounced photocurrent under illumination that started when −0.25 V was applied, and increased to 1.3 mA/cm^2 when +1.0 V was applied. The photocurrent density in ZnO nanorods that were loaded with Au nanoparticles (12 h) was about double that of pristine ZnO nanowires with a similar thickness (~0.7 mA/cm^2) at 1.0 V, suggesting that decoration by Au nanoparticles promoted the harvesting of solar light. As the deposition time was further increased, an important effect occurred. Most interestingly, the photocurrent declined greatly as the deposition time increased to 24 h. This result is particularly interesting. This phenomenon indicates that several effects originated from either the localized surface plasmon or the collection of sunlight, which was involved in the photoelectrochemical reaction on the Au−ZnO photoelectrode. Although the more loading amount of Au nanoparticles can lead to an increase in hot electrons injection and contribute a detectable photocurrent to an entire device (as shown in Figure 3b), the Au−ZnO

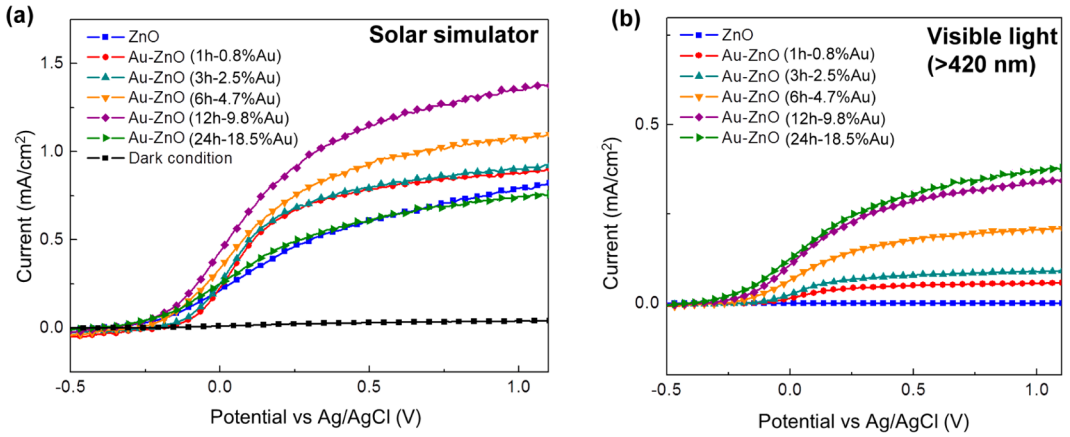

Figure 3. (a) Linear-sweep voltammograms of Au−ZnO photoelectrodes with nanoparticles deposited for various periods, and a dark scan, performed in a 0.5 M aqueous Na_2SO_4 with a pH of 6.8 under an AM 1.5 solar simulator. (b) Linear-sweep voltammograms of Au−ZnO photoelectrodes with nanoparticles deposited for various periods, obtained under illumination by visible light (>420 nm).

sample with 24 h of deposition exhibited a great decrease in its photocurrent. This may be attributed to the blocking effect of gold nanoparticles upon the ZnO nanorods, since the loading amount of the 24 h sample was almost twice as much as that of the 12 h depositon sample, indicating that Au nanoparticles upon the ZnO would block two times the irradiation from the solar simulator and suppress the photoexcitation process on ZnO, which was a UV active semiconductor. Therefore, metallic gold may also act as trap centers for photoelectrons and collect some photogenerating electrons from the ZnO nanorods; this phenomenon results in a negative effect in photoresponse. As a result, the sample with 12 h of deposition (~10% loading) was expected to be an optimum condition for both hot electron injection and light absorption of the semiconductor support.

To explore hot electron generation and plasmon damping, a Au−ZnO photoelectrode was irradiated with visible light (>420 nm) to eliminate the effects of the photoexcitation of ZnO. ZnO nanorods with a large bandgap of above 3 eV are a UV-photoactive material, such that the measured photoresponse under illumination by visible light (>420 nm) is attributable largely to plasmonic Au nanoparticles. Figure 3b presents a set of linear sweep voltammagrams of pristine ZnO nanorods and ZnO nanorods that were loaded with Au nanoparticles that had been deposited for various durations under illumination by visible light (>420 nm) with an intensity of 100 mW/cm^2. Pristine ZnO nanorods generate no obvious photocurrent because ZnO is inactive in the visible region. When a few Au nanoparticles decorate the array, the photocurrent depends substantially on the number of Au nanoparticles, reaching a maximum of 0.3 mA/cm^2. Further increasing the number of Au nanoparticles cannot significantly increase its photocurrent, suggesting that optimal decoration had been achieved and that further increasing the number of Au nanoparticles would not increase the measured photoresponse of the PEC by contributing more photoelectrons. This result is consistent with the *I*−*V* measurements under full-spectrum solar illumination and reveals that excess Au nanoparticles could not significantly contribute to the photoresponse but had a blocking effect that reduced the absorption of light by the ZnO nanorods. The photocurrent density of an Au−ZnO photoelectrode (12 h) increased with applied voltage, starting at −0.25 V *versus* Ag/AgCl, and reaching 0.3 mA/cm^2 at 1.0 V. It was similar to that of the Au−ZnO photoelectrode under a full-spectrum solar simulator (Figure 3a). We suggest that the hot electrons that are generated by plasmon damping under visible illumination can be injected into the ZnO over the Schottky barrier, yielding a detectable photocurrent under visible illumination. Notably, plasmonic enhancement is attributable to the injection of hot electrons from plasmonic materials into the conduction band of the semiconductor (ZnO) rather than to the trapping of photogenerating electrons from the conduction band of the semiconductor and their transfer and subsequent reaction with hydrogen ions. The transfer of photogenerated electrons from the conduction band of the semiconductor to the metal is energetically unfavorable because the photoelectrons must overcome the Schottky barrier even though this barrier is small.

Because of shape/size-dependent nature for gold nanostructure, Figure 4a displays the TEM image of as-prepared Au nanoparticles, which are small, with a mean diameter of 4.7 nm with a standard deviation of 0.7 nm. The TEM image (Figure 4b) of ZnO nanorods that are decorated with an ensemble of Au nanoparticles (12 h) reveals that these particles are uniformly distributed upon the surface and uniform in diameter. The distribution of Au nanoparticles on the surface of the ZnO nanorod may be optimal because more Au nanoparticles would have had a negative effect, blocking ZnO nanorods from absorbing solar illumination,

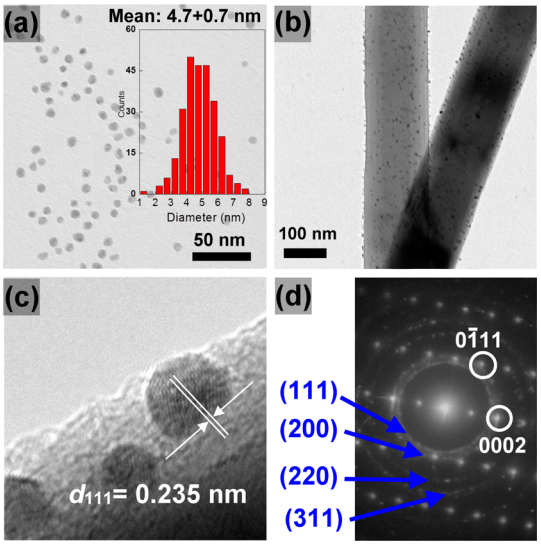

Figure 4. (a) TEM micrographs and distribution of sizes of as-prepared gold nanoparticles (12 h); (b) TEM micrographs and (c) high-resolution image of Au−ZnO photoelectrodes; (d) corresponding electron diffraction pattern of Au−ZnO photoelectrode.

suppressing the photogeneration process of ZnO under ultraviolet irradiation. A high-resolution TEM image of the edge of a nanorod (Figure 4c) provides more compelling evidence that Au nanoparticles are attached to its surface. An abrupt transition is observed between the lattice planes of the ZnO nanorod and the (111) lattice planes of the Au nanoparticles. The lattice spacing between the (111) planes, 0.235 nm, is also consistent with that of the gold bulk crystal (JCPDS no. 89-3697). Most interestingly, the selected electron diffraction pattern (Figure 4d) is characteristic of the two-component crystalline nature. The set of spot pattern can be indexed to the [$2\bar{1}\bar{1}0$] zone axis of the ZnO wurtzite structure zone axis, which is a single crystalline structure (indicated by the white circle). The set of rings reveals a typical face-centered-cubic polycrystalline structure that corresponds to bulk gold and is probably associated with the large amount of Au nanoparticles on the surface of the ZnO nanowires. These results indicate that Au nanoparticles were successfully attached to the surfaces of ZnO nanowires. The following section will systematically address the effects of localized surface plasmon upon the ZnO nanorods and their relationship to the water splitting reaction.

Plasmon-Induced Hot Electron−Hole Pairs. To clarify the mechanism of localized plasmon-induced enhancement, several competing processes for plasmon resonance damping processes are considered. The first important property of plasmon damping is the nonradiative decay of plasmon owing to the generation of electron−hole pairs by either intraband excitation within the conduction band or interband transition from a lower-lying d band to the sp conduction band.[52]

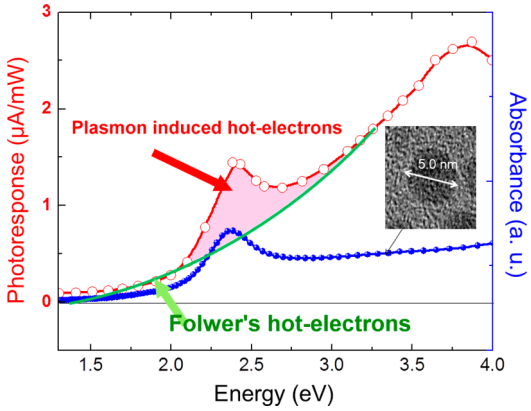

Figure 5. Absorption spectrum of Au nanospheres and plots of photocurrent *versus* wavelength, fitted to Fowler's law, indicating that photocurrent comprises mainly hot electron flow, with additional contribution from hot electrons that are injected from Au under plasmonic-induced irradiation that is amplified by localized surface plasmon resonance.

This process of "hot" electron generation has been demonstrated and measured in solid-state devices,[53] but it has remained unexploited in photoelectrochemical cells. To confirm the relationship between hot electron flux and plasmon damping, the photocurrent in the PEC was measured as a function of the wavelength of light (Figure 5). The number of photoelectrons that had sufficient energy to overcome the barrier is given by the Fowler theory:

$$\eta_i = C_F \frac{(h\upsilon - \phi)^n}{h\upsilon}$$

where C_F is the Fowler emission coefficient;[53] $n = 2$ for most metals, and φ is the Schottky barrier energy. Figure 5 also plots the photocurrent fitted using Fowler's law with parameters $n = 2$ and $\varphi = 0.7$ eV. Since a bias of 0.5 V was applied to this system, the Schottky barrier should be 1.2 eV with zero bias, which is consistent with the value that was obtained by fitting. This result demonstrates that photocurrent is mainly associated with hot electron flow. Specifically, the photocurrent diverges from Fowler's law, indicating a significant contribution of the injection of hot electrons associated with Au plasmonic resonance (as indicated in Figure 5), revealing that localized surface plasmon resonance can promote hot electron flow. To verify the presence of a localized surface plasmon effect, absorption spectra were obtained. The spectrum of the Au nanospheres includes a strong plasmon resonance band in the visible region, as was identical to that observed in Figure 5. Au nanoparticles considerably increase the photocurrent in a PEC owing to their surface plasmon band, which enables them to generate hot electrons that contribute to the photo response of photoelectrochemical cell beyond Fowler emission. The Au−ZnO photoelectrode was further tested under on−off cycle illumination conditions to

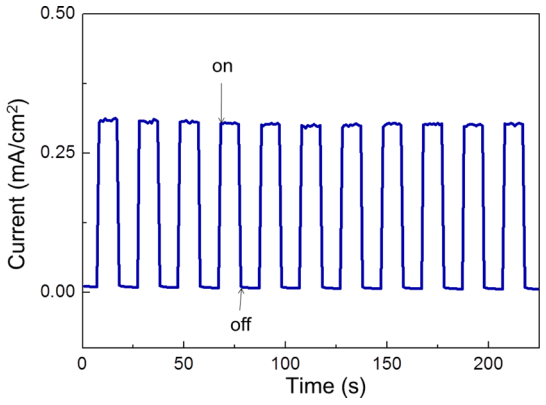

Figure 6. Amperometric *I*−*t* curves of Au−ZnO photoelectrode (12 h) with on/off cycles under a solar simulator with an intensity of 100 mW/cm^2.

determine whether the measured photocurrent was associated with the absorption of light. Figure 6 plots the photocurrent that is generated by the injection of hot electrons for an Au−ZnO photoelectrode under visible light. Upon illumination, a spike in the photoresponse (~0.3 mA/cm^2) was observed owing to the transient effect during excitation, and the photocurrent rapidly returned thereafter to a steady state.[47,54] This result further verifies that photogenerated electrons are rapidly transported from Au nanoparticles to ZnO nanowires.

Plasmon-Induced Electromagnetic Field. Another possible cause of the enhancement of photocurrent is the plasmon-induced electromagnetic field. Although an earlier study proposed that an electromagnetic field may contribute to photoactivity,[33] the effects of the plasmon-induced electromagnetic field have not been experimentally elucidated. Since the photochemical property of the water splitting reaction is greatly dependent on the band structure of the semiconductor, we suggest that the plasmon-induced electromagnetic field may modify the valence/conduction bands of ZnO and determine its photoactivity. Therefore, XAS was utilized to provide valuable evidence of the structural parameter and electronic structure of Zn atoms,[38,41] and *in situ* measurements were made simultaneously to collect the spectra with/without illumination at the desired wavelength. Further monochromatic incident light was applied to induce localized plasmonic effects upon the Au nanostructures, which were involved in the chemical reaction, and facilitated an exploration of the metal/semiconductor interface, and the interaction of all of these with chemical reactants. To provide further insight into the interface between ZnO and the gold nanostructures and to elucidate the influence of a plasmon-induced electromagnetic field upon the surfaces of ZnO, the densities of states (DOS) of the ZnO was calculated using density function theory (DFT). The ultimate goal was to elucidate the evolution of the electronic structure.[55] As displayed in Figure 7a, the conduction band comprises mainly the Zn_{4s}+ Zn_{4p} states and the valence band is composed of the O_{2p} state. The X-ray absorption near edge structure (XANES) of the Zn K-edge is used to elucidate the structure of the conduction band of ZnO since the K-edge absorption involves the transition from the 1s to 4p states, such that a higher XANES intensity indicates the presence of more vacant 4p states and more vacancies in the conduction band of ZnO. The region that is affected by the plasmon-induced field can be easily determined to be smaller than several tens of nanometers. Importantly, the XAS of Zn K-edge is obtained *via* the fluorescence emission, since sampling deep of fluorescence emission is below 100 nm, which means we can conduct the local modification near the surface of ZnO to attain the extract evolution from plasmon-induced effects. The difference between the XANES of bare ZnO nanorods and that of the Au−ZnO photoelectrode yielded the relative vacancy ($\Delta A/A$) on the conduction band (as shown in Figure 7).[43] Compare to ZnO (dark condition), the amount of relative vacancy observably decreased as ZnO nanorods absorbed UV irradiation. This phenomenon is attributed to generation of photoelectrons in the conduction band and the occupancy of the 4p state in Zn when ZnO was irradiated by UV. It reduced the number of vacancies and revealed the photogeneration process of ZnO under a UV irradiation (380 nm). When ZnO nanorods were decorated with gold nanoparticles (without illumination), the relative vacancy slightly exceeded that of pristine ZnO nanorods owing to the realignment of the Fermi levels between the gold nanoparticle/ZnO nanorod interface. The large increase vacancies under plasmon-induced illumination (530 nm) demonstrated that localized surface plasmon resonance significantly modified the electronic structure of ZnO and generated more vacancies in the conduction band. Notably, irradiation at 530 nm (2.33 eV) provided sufficient energy to generate hot electrons that flowed from gold to the conduction band of ZnO through the Schottky barrier (~1.2 eV), as elucidated above. However, plasmon resonance still has the positive effect of generating more vacancies in CB despite a flow of hot electrons into the conduction band of ZnO. Localized surface plasmon resonance can generate a strong electromagnetic field close to the surfaces of gold nanoparticles when plasmon-induced illumination is applied to the photoelectrode. This field modifies the band structure at the Au/ZnO interface, resulting in rapid transportation of photogenerated electron−hole pairs.

Plasmon-Induced Heating. The third plasmonic effect, heat generation, under illumination at plasmonic resonance should be considered.[56] The finite-difference time-domain (FDTD) program, MEEP, has also been used to calculate induced heat from gold nanoparticles.[56] The energy that flows out through the boundary surfaces of volume *V* per unit time plus the

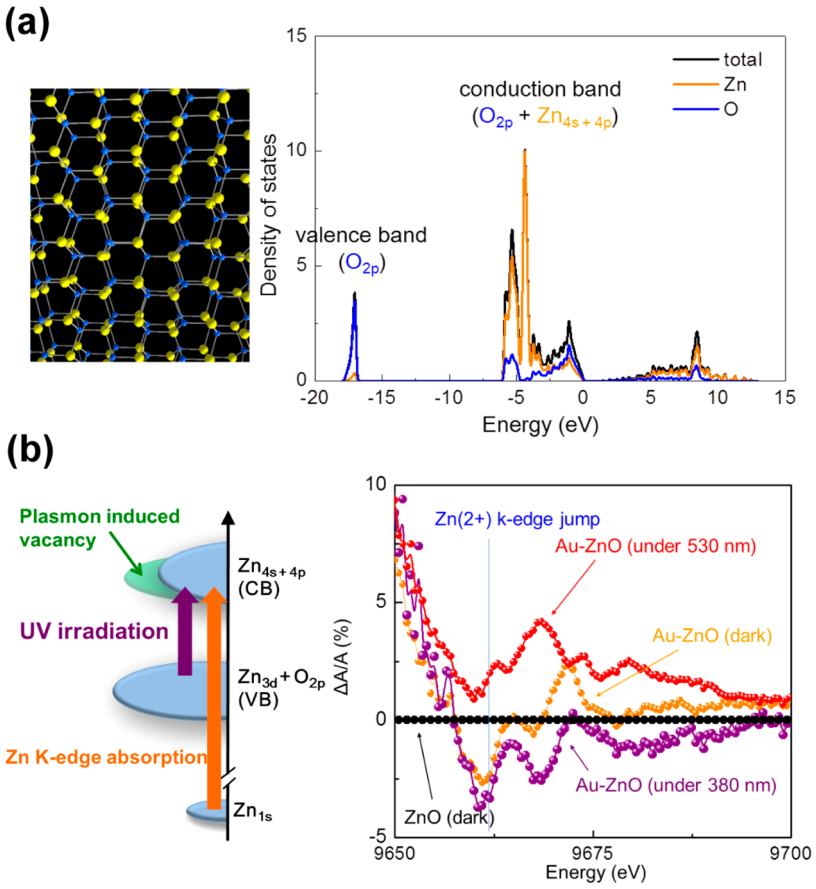

Figure 7. (a) Density of states for ZnO calculated by density function theory; (b) relative vacancies for ZnO rods (dark condition), ZnO rods (@ UV illumination), Au−ZnO (dark condition), Au−ZnO (@ 530 nm illumination).

rate of energy loss by absorptive dissipation in the volume equals the negative rate of change in electromagnetic energy within the volume.[57] When the medium is not magnetically dispersive, the time-averaged dissipative energy density can be reduced as[56]

$$q = q_e = \frac{1}{2}\varepsilon_0 \omega \, \mathrm{Im}\varepsilon(\omega)|E|^2$$

Accordingly, the energy of the absorbed light in the system herein that is converted to heat (Q) is

$$Q = \int_V q \, dV$$

This equation is used to calculate the heat generated by a single gold sphere with a diameter of 5 nm (Q_{sphere}), which is 6.97×10^{-20} J. On the basis of the elemental analysis and an operated systematic calculation (in the Supporting Information), it is estimated that Au nanoparticles of approximately 9.8×10^{-2} mg are present on the photoelectrode and the total heat generation from the Au nanoparticles is about 9.72×10^{-7} J, which indicates rhat the heat generation cannot significantly influence the system temperature or the water splitting reaction herein (Figure 8a Supporting Information, Tables S1 and S2), and all measurements were made at a controlled temperature of 25 °C. To explain this effect further, the relative vacancies of ZnO nanorods at various temperatures are determined to elucidate the evolution of the electronic structure in Zn. As presented in Figure 8b, the relative vacancy desired temperature was similar to that even above 100 °C, indicating that heating could not strongly affect the electronic properties of ZnO nanorods. As a result, any contribution from plasmon-induced heat can be ruled out.

The time course of Au−ZnO photoelectrode (12 h, 9.8% Au) for overall water splitting is presented in Figure 9. About 11.2 and 4.4 μmol h^{-1} of H_2 and O_2 molecules were generated by the Au−ZnO photoelectrodes under irradiation by AM 1.5 illumination, in which the Faraday efficiencies were 86% and 69%, respectively. Notably, the Faraday efficiency of Au−ZnO photoelectrode for hydrogen evolution is greater than that of oxygen evolution, this phenomenon can be attributed to surface catalytic effect.[58] The platinum foil was applied as a counter-electrode that has been demonstrated to significantly catalyze the hydrogen evolution in an electrochemical cell. Compared to a bare ZnO nanorod photoanode, a Au−ZnO photoanode has revealed that plasmon induced effects can

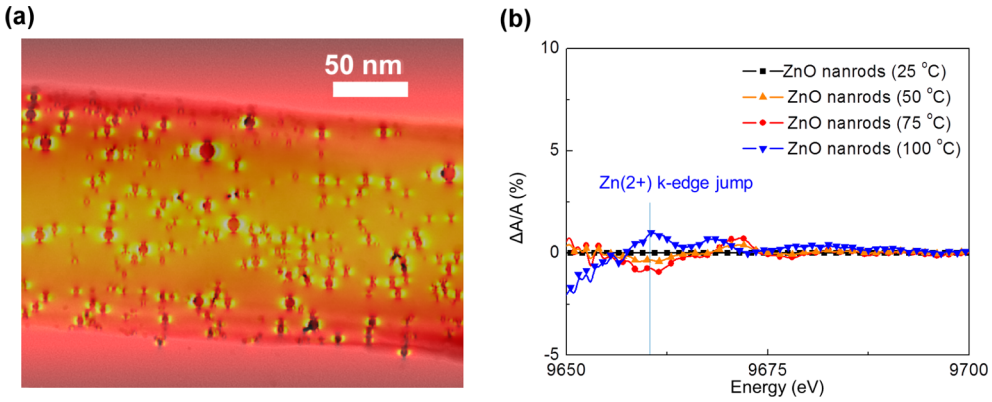

Figure 8. (a) Simulated heat generation distribution map of Au nanospheres−ZnO nanorod (12 h); (b) relative vacancies of Au−ZnO photoelectrode at desired temperature.

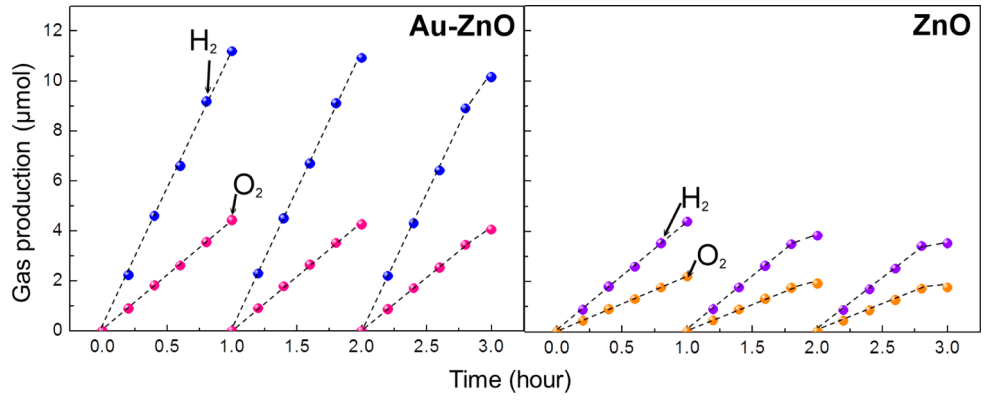

Figure 9. Time courses of H_2 and O_2 evolution using Au−ZnO and ZnO photoelectrodes under AM 1.5G solar simulator in 0.5 M Na_2SO_4 aqueous solution.

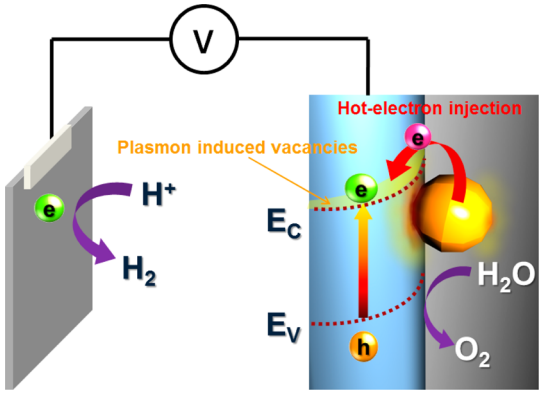

Figure 10. Schematic illustration of the plasmon-induced effects on Au−ZnO photoelectrode.

significantly enhance the overall water splitting. This successful realization of a plasmonic induced mechanism under the irradiation of sunlight led to exceptional performance in the photocatalytic evolution of hydrogen and oxygen.

Figure 10 presents a model mechanism of the enhancement by localized surface plasmon resonance on an Au nanostructure. When the photoanode (Au−ZnO photoelectrode) captured solar illumination and ZnO simultaneously generated photoelectrons, the photogenerated electrons migrated to the conduction band of ZnO. Simultaneously, the Au nanostructure absorbed plasmon-induced irradiation, generating hot electrons and an electromagnetic field. The plasmon-induced hot electrons were injected into the conduction band of ZnO over the Schottky barrier, and they were driven to the photocathode, where they reacted with protons to form hydrogen, in which excited Au nanoparticles can generate holes to accept electrons from electrolyte (water) and form oxygen.[59] With the progression of the plasmon hot-electron injection, excited Au nanoparticles may form a plasmon-induced reaction with water to evolve hydrogen and oxygen. The plasmon-induced electromagnetic field creates additional vacancies at the bottom of the conduction band, facilitating the generation of photoelectrons by photoexcitation. The plasmon-induced electromagnetic fields are spatially nonhomogenous and strong close to the plasmon materials, suggesting that the formation of electron−hole pairs should be greatest in the part of the semiconductor that is the closest to the gold nanostructures. This formation of a highly electromagnetic region close to the semiconductor surface rather than in the bulk has

several advantages. The electron–hole pairs are readily separated under the influence of the surface potential and their distance to travel to the surface of ZnO, where they can react with water in a photochemical reaction, is shortened. Accordingly, the coupling of hot electrons that are formed by the plasmon with the electromagnetic field has several effects, effectively enhancing the probability of the photochemical reaction associated in the splitting of water.

CONCLUSIONS

This work demonstrated plasmon-induced effects on an array of Au nanostructure–ZnO nanorods as a photoanode. Several strategies were successfully utilized to identify the independent contributions from various plasmonic effects under solar irradiation, explaining why the coupling of hot electrons that were formed by plasmons with the electromagnetic field effectively increases the probability of the photochemical reaction in the splitting of water. The hot electrons that are generated by the plasmons are injected from the plasmonic materials into the conduction band of the semiconductor, while the plasmon-induced electromagnetic field creates vacancies in the conduction band of the surface of ZnO, promoting the separation of photogenerated electrons and holes. The photocatalysts of greatest research interest are n-type semiconductors, but the demonstration herein of Au nanospheres and ZnO nanorods with n-type semiconductor characteristics should be able to be extended easily to other photochemical systems.

The results herein demonstrate a new approach to investigating localized plasmon-induced effects and charge separation in photoelectrochemical process. Localized plasmon resonance has recently been exploited to enhance significantly the photochemical processes in photovoltaic devices, but the details of the mechanism remain unclear. Further study on plasmon enhancement remain to be progressed and optimized, cocatalyst loading with plasmonic materials for both photocathode and photoanode may be an alternative direction for improving their efficiency of solar water splitting. In terms of particle size, larger size would lead to an undesired effect in photoresponse, in which plasmonic nanoparticles block light absorption of semiconductors and suppress the photoactivity of semiconductor. Small size may be a proper and optimum condition for both plasmon-induced effects and overall photoactivity. Therefore, many factors should be considered in choosing a promising material, such as stability in electrolyte, interface of plasmonics/semiconductor, plasmon resonance wavelength, and shapes/sizes. Although solar water splitting has been used as platform to elucidate the mechanism of surface plasmon resonance, we believe that the strategies herein and the presented understanding of how photogenerated electrons are transferred are fundamental to the design of energy conversion devices and become a general viewpoint for many plasmonic enhancements.

MATERIALS AND METHODS

Chemicals and Substrates. Zinc acetate [$Zn(CH_3CO_2)_2$], absolute ethanol, and zinc nitrate [$Zn(NO_3)_2$] were purchased from Sigma-Aldrich. Hydrogen tetrachloroaurate (III) hydrate ($HAuCl_4$), hexamethylenetetramine (HMT), and trisodium citrate dihydrate ($C_6H_5Na_3O_7 \cdot 2H_2O$) were purchased from Across Organics, and mercaptopropionic acid (MPA) was purchased from Fluka. All chemicals were used as delivered and without further purification. The water that was used throughout this investigation was reagent-grade, and produced using a Milli-Q SP ultrapure water purification system from Nihon Millipore Ltd., Tokyo. Fluorine-doped tin oxide substrates (F:SnO_2, 10 Ω/□) were purchased from Hartford Glass Company.

Synthesis of ZnO Nanorods. First, F:SnO_2 (FTO) was cleaned by ultrasonic agitation in acetone and an ethanol bath for 10 min. A 100 mL aliquot of 0.1 M zinc acetate in absolute ethanol was prepared to form seeds. The FTO substrates were dipped into zinc acetate solution for 10 s and then blown dry in a stream of argon. This process was repeated eight times. Finally, the substrates were calcined at 350 °C for 30 min in air to yield a thin layer of ZnO seeds. The seeded substrates were then suspended horizontally in a reagent solution that contained 0.06 M zinc nitrate and 0.06 M hexamethylenetetramine in a Teflon vessel. The Teflon vessel was sealed in an autoclave and heated to initiate nanorod growth at 110 °C for 24 h. The rate of nanowire growth was approximately 0.2 μm per hour. The nanowire substrate was removed from the autoclave, thoroughly washed using D.I. water, and then dried in an atmosphere of air. Further annealing at 450 °C for 30 min in the atmosphere of air was critical to improve the crystallinity of the ZnO nanorods.

Synthesis of Gold Nanoparticles. Water was used as the solvent in all reactions, in which sodium citrate acted as both the capping reagent and the reducing agent. In a typical preparation, the colloidal nanoparticles were prepared by adding 5 mL of sodium citrate (1%) to 50 mL of gold metal salt ($HAuCl_4$, 0.4 mM) solution. The solution was heated at 95 °C in an oil bath for 15 min, and then allowed to cool before the subsequent experiment was carried out.

Preparation of Photoeletrode. The as-prepared ZnO nanorod array substrates were placed with their nanowire side up in a gold nanoparticle solution for the desired duration. Following deposition in a chemical bath, the substrate was removed from the solution and washed by deionized (D.I.) water to remove any excess gold solution. This gold-decorated ZnO substrate was connected to a copper wire using silver paste and dried overnight. The substrate and wire were subsequently covered with insulating epoxy exposing only the desired surface area.

Photoelectrochemical Characterization. The electrochemical characterization was carried out using three electrode-based methods. An Au–ZnO photoelectrode was the working electrode; an Ag/AgCl electrode was the reference electrode, in which the platinum plate was the counter electrode. All photoelectrochemical cells (PEC) were examined in 0.5 M Na_2SO_4 (pH = 6.8) solution, which served as the supporting electrolyte, and the photoelectrode was illuminated with a xenon lamp that was equipped with AM 1.5 filter. The I–V characteristic of the PEC was recorded using a potentiostat (Eco Chemie AUTOLAB (The Netherlands)) and GPES (general Purpose Electrochemical System) software at 25 °C. The gas evolution was conducted in the same condition with a bias of +0.5 V.

Simulation. Gold nanorods ($\varepsilon_m = -4.47643 + 2.53177i$), zinc oxide (ZnO) ($\varepsilon_d = 1.95908$), and the surrounding material (H_2O)

(n = 1.33) were utilized and electric field intensity was determined by calculating three-dimensional Maxwell equations with commercial solver COMSOL Multiphysics 3.5a, which is based on the finite element method (FEM). All of the boundaries were set as periodic boundary conditions such that the layers were matched to a large number of gold nanoparticles in water. The finite-difference time-domain (FDTD) program, MEEP, has also been used to calculate induced heat from gold nanoparticles. In this simulation, all of the boundary conditions were set such that the layers were perfectly matched to eliminate interference of refracted waves with the incident light. The x, y, and z dimensions of the grid cells are all 1 nm. The boundary conditions are all set as perfect.

Characterization of Materials. High-resolution transmission electron microscope (HRTEM) images, electron diffraction patterns, and elemental maps were obtained under a JEOL JEM-2100F electron microscope. The morphology of the nanowires was elucidated with a JEOL JSM-6700F field-emission scanning electron microscope (FESEM). A series of XAS measurements of the synthesized samples were made using synchrotron radiation at room temperature. Measurements were made at the Zn K-edge (9.659 keV) with the sample held and illuminated by the light of interest at room temperature. The experiments were conducted at the 01C1 beamline of the National Synchrotron Radiation Research Center (NSRRC), Taiwan.

Conflict of Interest: The authors declare no competing financial interest.

Acknowledgment. The authors gratefully acknowledge the financial support of the National Science Council of Taiwan (Contracts Nos. NSC 101-2113-M-002-014-MY3, 101-3113-P-002-021, 100-2923-M-002-007-MY3, 101-2112-M-002-023). They are also grateful to the National Center for Theoretical Sciences, Taipei Office, the Molecular Imaging Center of National Taiwan University, and the National Center for High-Performance Computing, Taiwan, for their support.

Supporting Information Available: Cross-section SEM image of ZnO nanorods, SEM images of Au−ZnO photoelectrodes with nanoparticles deposited for various periods, absorption spectrum of Au nanoparticles, spectrum of solar simulator, elemental analysis of Au−ZnO photoelectrodes, and heat generation of gold nanospheres. This material is available free of charge *via* the Internet at http://pubs.acs.org.

REFERENCES AND NOTES

1. Zhu, J.; Cui, Y. More Solar Cells for Less. *Nat. Mater.* **2010**, *9*, 183–184.
2. Yoon, T. P.; Ischay, M. A.; Du, J. Visible Light Photocatalysis as a Greener Approach to Photochemical Synthesis. *Nat. Chem.* **2010**, *2*, 527–532.
3. Listorti, A.; Durrant, J.; Barber, J. Solar to Fuel. *Nat. Mater.* **2009**, *8*, 929–930.
4. Allam, N. K.; Poncheri, A. J.; El-Sayed, M. A. Vertically Oriented Ti−Pd Mixed Oxynitride Nanotube Arrays for Enhanced Photoelectrochemical Water Splitting. *ACS Nano* **2011**, *5*, 5056–5066.
5. Hartmann, P.; Lee, D.-K.; Smarsly, B. M.; Janek, J. Mesoporous TiO_2: Comparison of Classical Sol-Gel and Nanoparticle Based Photoelectrodes for the Water Splitting Reaction. *ACS Nano* **2010**, *4*, 3147–3154.
6. Meyer, T. J. The Art of Splitting Water. *Nature* **2008**, *451*, 778–779.
7. Dang, X.; Yi, H.; Ham, M.-H.; Qi, J.; Yun, D. S.; Ladewski, R.; Strano, M. S.; Hammond, P. T.; Belcher, A. M. Virus-Templated Self-Assembled Single-Walled Carbon Nanotubes for Highly Efficient Electron Collection in Photovoltaic Devices. *Nat. Nanotechnol.* **2011**, *6*, 377–384.
8. Yi, Z. G.; Ye, J. H.; Kikugawa, N.; Kako, T.; Ouyang, S. X.; Stuart-Williams, H.; Yang, H.; Cao, J. Y.; Luo, W. J.; Li, Z. S.; *et al.* An Orthophosphate Semiconductor with Photooxidation Properties under Visible-Light Irradiation. *Nat. Mater.* **2010**, *9*, 559–564.
9. Chen, X. B.; Shen, S. H.; Guo, L. J.; Mao, S. S. Semiconductor-Based Photocatalytic Hydrogen Generation. *Chem. Rev.* **2010**, *110*, 6503–6570.
10. Walter, M. G.; Warren, E. L.; McKone, J. R.; Boettcher, S. W.; Mi, Q. X.; Santori, E. A.; Lewis, N. S. Solar Water Splitting Cells. *Chem. Rev.* **2010**, *110*, 6446–6473.
11. Kudo, A.; Miseki, Y. Heterogeneous Photocatalyst Materials for Water Splitting. *Chem. Soc. Rev.* **2009**, *38*, 253–278.
12. Chen, H. M.; Chen, C. K.; Liu, R.-S.; Zhang, L.; Zhang, J.; Wilkinson, D. P. Nano-Architecture and Material Designs for Water Splitting Photoelectrodes. *Chem. Soc. Rev.* **2012**, 10.1039/C2CS35019J.
13. Bang, J. H.; Kamat, P. V. Quantum Dot Sensitized Solar Cells. A Tale of Two Semiconductor Nanocrystals: CdSe and CdTe. *ACS Nano* **2009**, *3*, 1467–1476.
14. Buhbut, S.; Itzhakov, S.; Tauber, E.; Shalom, M.; Hod, I.; Geiger, T.; Garini, Y.; Oron, D.; Zaban, A. Built-in Quantum Dot Antennas in Dye-Sensitized Solar Cells. *ACS Nano* **2010**, *4*, 1293–1298.
15. Wang, X. N.; Zhu, H. J.; Xu, Y. M.; Wang, H.; Tao, Y.; Hark, S.; Xiao, X. D.; Li, Q. A. Aligned ZnO/CdTe Core−Shell Nanocable Arrays on Indium Tin Oxide: Synthesis and Photoelectrochemical Properties. *ACS Nano* **2010**, *4*, 3302–3308.
16. Zhang, J.; Bang, J. H.; Tang, C. C.; Kamat, P. V. Tailored TiO_2−$SrTiO_3$ Heterostructure Nanotube Arrays for Improved Photoelectrochemical Performance. *ACS Nano* **2010**, *4*, 387–395.
17. Chen, H. M.; Liu, R. S. Architecture of Metallic Nanostructures: Synthesis Strategy and Specific Applications. *J. Phys. Chem. C* **2011**, *115*, 3513–3527.
18. Tao, A. R.; Habas, S.; Yang, P. Shape Control of Colloidal Metal Nanocrystals. *Small* **2008**, *4*, 310–325.
19. Halas, N. J.; Lal, S.; Chang, W. S.; Link, S.; Nordlander, P. Plasmons in Strongly Coupled Metallic Nanostructures. *Chem. Rev.* **2011**, *111*, 3913–3961.
20. Oulton, R. F.; Sorger, V. J.; Zentgraf, T.; Ma, R.-M.; Gladden, C.; Dai, L.; Bartal, G.; Zhang, X. Plasmon Lasers at Deep Subwavelength Scale. *Nature* **2009**, *461*, 629–632.
21. Okamoto, K.; Niki, I.; Shvartser, A.; Narukawa, Y.; Mukai, T.; Scherer, A. Surface-Plasmon-Enhanced Light Emitters Based on InGaN Quantum Wells. *Nat. Mater.* **2004**, *3*, 601–605.
22. Luk'yanchuk, B.; Zheludev, N. I.; Maier, S. A.; Halas, N. J.; Nordlander, P.; Giessen, H.; Chong, C. T. The Fano Resonance in Plasmonic Nanostructures and Metamaterials. *Nat. Mater.* **2010**, *9*, 707–715.
23. Kaelberer, T.; Fedotov, V. A.; Papasimakis, N.; Tsai, D. P.; Zheludev, N. I. Toroidal Dipolar Response in a Metamaterial. *Science* **2010**, *330*, 1510–1512.
24. Stockman, M. Nanofocusing of Optical Energy in Tapered Plasmonic Waveguides. *Phys. Rev. Lett.* **2004**, *93*, 137404.
25. Maier, S. A.; Kik, P. G.; Atwater, H. A.; Meltzer, S.; Harel, E.; Koel, B. E.; Requicha, A. A. G. Local Detection of Electromagnetic Energy Transport below the Diffraction Limit in Metal Nanoparticle Plasmon Waveguides. *Nat. Mater.* **2003**, *2*, 229–232.
26. Bukasov, R.; Ali, T. A.; Nordlander, P.; Shumaker-Parry, J. S. Probing the Plasmonic Near-Field of Gold Nanocrescent Antennas. *ACS Nano* **2010**, *4*, 6639–6650.
27. Slaughter, L. S.; Wu, Y. P.; Willingham, B. A.; Nordlander, P.; Link, S. Effects of Symmetry Breaking and Conductive Contact on the Plasmon Coupling in Gold Nanorod Dimers. *ACS Nano* **2010**, *4*, 4657–4666.
28. Zuloaga, J.; Prodan, E.; Nordlander, P. Quantum Plasmonics: Optical Properties and Tunability of Metallic Nanorods. *ACS Nano* **2010**, *4*, 5269–5276.
29. Anderson, L. J. E.; Payne, C. M.; Zhen, Y. R.; Nordlander, P.; Hafner, J. H. A Tunable Plasmon Resonance in Gold Nanobelts. *Nano Lett.* **2011**, *11*, 5034–5037.
30. Ye, J.; Wen, F. F.; Sobhani, H.; Lassiter, J. B.; Van Dorpe, P.; Nordlander, P.; Halas, N. J. Plasmonic Nanoclusters: Near Field Properties of the Fano Resonance Interrogated with SERS. *Nano Lett.* **2012**, *12*, 1660–1667.
31. Gao, H.; Liu, C.; Jeong, H. E.; Yang, P. Plasmon-Enhanced Photocatalytic Activity of Iron Oxide on Gold Nanopillars. *ACS Nano* **2012**, *6*, 234–240.
32. Brillet, J.; Gratzel, M.; Sivula, K. Decoupling Feature Size and Functionality in Solution-Processed, Porous Hematite

Electrodes for Solar Water Splitting. *Nano Lett.* **2010**, *10*, 4155–4160.
33. Liu, Z.; Hou, W.; Pavaskar, P.; Aykol, M.; Cronin, S. B. Plasmon Resonant Enhancement of Photocatalytic Water Splitting under Visible Illumination. *Nano Lett.* **2011**, *11*, 1111–1116.
34. Thomann, I.; Pinaud, B. A.; Chen, Z.; Clemens, B. M.; Jaramillo, T. F.; Brongersma, M. L. Plasmon Enhanced Solar-to-Fuel Energy Conversion. *Nano Lett.* **2011**, *11*, 3440–3446.
35. Furube, A.; Du, L.; Hara, K.; Katoh, R.; Tachiya, M. Ultrafast Plasmon-Induced Electron Transfer from Gold Nanodots into TiO_2 Nanoparticles. *J. Am. Chem. Soc.* **2007**, *129*, 14852–14853.
36. Yu, J. G.; Dai, G. P.; Huang, B. B. Fabrication and Characterization of Visible-Light-Driven Plasmonic Photocatalyst $Ag/AgCl/TiO_2$ Nanotube Arrays. *J. Phys. Chem. C* **2009**, *113*, 16394–16401.
37. Nishijima, Y.; Ueno, K.; Yokota, Y.; Murakoshi, K.; Misawa, H. Plasmon-Assisted Photocurrent Generation from Visible to Near-Infrared Wavelength Using a Au-Nanorods/TiO_2 Electrode. *J. Phys. Chem. Lett.* **2010**, *1*, 2031–2036.
38. Chen, H. M.; Hsin, C. F.; Chen, P. Y.; Liu, R. S.; Hu, S.-F.; Huang, C.-Y.; Lee, J.-F.; Jang, L.-Y. Ferromagnetic $CoPt_3$ Nanowires: Structural Evolution from fcc to Ordered $L1_2$. *J. Am. Chem. Soc.* **2009**, *131*, 15794–15801.
39. Chen, H. M.; Hsin, C. F.; Liu, R. S.; Lee, J.-F.; Jang, L.-Y. Synthesis and Characterization of Multi-pod-shaped Gold/Silver Nanostructures. *J. Phys. Chem. C* **2007**, *111*, 5909–5914.
40. Chen, H. M.; Liu, R. S.; Asakura, K.; Jang, L.-Y.; Lee, J.-F. Controlling Length of Gold Nanowires with Large-Scale: X-ray Absorption Spectroscopy Approaches to the Growth Process. *J. Phys. Chem. C* **2007**, *111*, 18550–18557.
41. Chen, H. M.; Liu, R. S.; Lo, M.-Y.; Chang, S.-C.; Tsai, L.-D.; Peng, Y.-M.; Lee, J.-F. Hollow Platinum Spheres with Nanochannels: Synthesis and Enhanced Catalysis for Oxygen Reduction. *J. Phys. Chem. C* **2008**, *112*, 7522–7526.
42. Chen, H. M.; Chen, C. K.; Lin, C. C.; Liu, R. S.; Yang, H.; Chang, W.-S.; Chen, K.-H.; Chan, T.-S.; Lee, J.-F.; Tsai, D. P. Multi-Bandgap-Sensitized ZnO Nanorod Photoelectrode Arrays for Water Splitting: An X-ray Absorption Spectroscopy Approach for the Electronic Evolution under Solar Illumination. *J. Phys. Chem. C* **2011**, *115*, 21971–21980.
43. Chen, H. M.; Chen, C. K.; Liu, R. S.; Wu, C.-C.; Chang, W.-S.; Chen, K.-H.; Chan, T.-S.; Lee, J.-F.; Tsai, D. P. A New Approach to Solar Hydrogen Production: A ZnO–ZnS Solid Solution Nanowire Array Photoanode. *Adv. Energy Mater.* **2011**, *1*, 742–747.
44. Chen, H. M.; Chen, C. K.; Chang, Y. C.; Tsai, C. W.; Liu, R. S.; Hu, S. F.; Chang, W. S.; Chen, K. H. Quantum Dot Monolayer Sensitized ZnO Nanowire-Array Photoelectrodes: True Efficiency for Water Splitting. *Angew. Chem., Int. Ed.* **2010**, *49*, 5966–5969.
45. Hochbaum, A. I.; Yang, P. D. Semiconductor Nanowires for Energy Conversion. *Chem. Rev.* **2010**, *110*, 527–546.
46. Fan, Z.; Razavi, H.; Do, J.-W.; Moriwaki, A.; Ergen, O.; Chueh, Y.-L.; Leu, P. W.; Ho, J. C.; Takahashi, T.; Reichertz, L. A.; *et al*. Three-Dimensional Nanopillar-Array Photovoltaics on Low-Cost and Flexible Substrates. *Nat. Mater.* **2009**, *8*, 648–653.
47. Law, M.; Greene, L. E.; Johnson, J. C.; Saykally, R.; Yang, P. D. Nanowire Dye-Sensitized Solar Cells. *Nat. Mater.* **2005**, *4*, 455–459.
48. Varghese, O. K.; Paulose, M.; Grimes, C. A. Long Vertically Aligned Titania Nanotubes on Transparent Conducting Oxide for Highly Efficient Solar Cells. *Nat. Nanotechnol.* **2009**, *4*, 592–597.
49. Dreaden, E. C.; Alkilany, A. M.; Huang, X. H.; Murphy, C. J.; El-Sayed, M. A. The Golden Age: Gold Nanoparticles for Biomedicine. *Chem. Soc. Rev.* **2012**, *41*, 2740–2779.
50. Ringe, E.; McMahon, J. M.; Sohn, K.; Cobley, C.; Xia, Y. N.; Huang, J. X.; Schatz, G. C.; Marks, L. D.; Van Duyne, R. P. Unraveling the Effects of Size, Composition, and Substrate on the Localized Surface Plasmon Resonance Frequencies of Gold and Silver Nanocubes: A Systematic Single-Particle Approach. *J. Phys. Chem. C* **2010**, *114*, 12511–12516.
51. Kelly, K. L.; Coronado, E.; Zhao, L. L.; Schatz, G. C. The Optical Properties of Metal Nanoparticles: The Influence of Size, Shape, and Dielectric Environment. *J. Phys. Chem. B* **2003**, *107*, 668–677.
52. Maier, S. A. Localized Surface Plasmons. In *Plasmonics: Fundamentals and Applications*; Springer: New York, 2006; pp 65–88.
53. Knight, M. W.; Sobhani, H.; Nordlander, P.; Halas, N. J. Photodetection with Active Optical Antennas. *Science* **2011**, *332*, 702–704.
54. Ahn, K. S.; Yan, Y.; Shet, S.; Jones, K.; Deutsch, T.; Turner, J.; Al-Jassim, M. ZnO Nanocoral Structures for Photoelectrochemical Cells. *Appl. Phys. Lett.* **2008**, *93*, 163117.
55. He, S.; Zhang, S. T.; Lu, J.; Zhao, Y. F.; Ma, J.; Wei, M.; Evans, D. G.; Duan, X. Enhancement of Visible Light Photocatalysis by Grafting ZnO Nanoplatelets with Exposed (0001) Facets onto a Hierarchical Substrate. *Chem. Commun.* **2011**, *47*, 10797–10799.
56. Hao, J.; Zhou, L.; Qiu, M. Nearly Total Absorption of Light and Heat Generation by Plasmonic Metamaterials. *Phys. Rev. B* **2011**, 83.
57. Jackson, J. D. *Classical Electrodynamics*; John Wiley & Sons: New York, 2001.
58. Maeda, K.; Xiong, A. K.; Yoshinaga, T.; Ikeda, T.; Sakamoto, N.; Hisatomi, T.; Takashima, M.; Lu, D. L.; Kanehara, M.; Setoyama, T.; *et al*. Photocatalytic Overall Water Splitting Promoted by Two Different Cocatalysts for Hydrogen and Oxygen Evolution under Visible Light. *Angew. Chem., Int. Ed.* **2010**, *49*, 4096–4099.
59. Tian, Y.; Tatsuma, T. Mechanisms and Applications of Plasmon-Induced Charge Separation at TiO_2 Films Loaded with Gold Nanoparticles. *J. Am. Chem. Soc.* **2005**, *127*, 7632–7637.